Preliminary Investigation of Polarization Effects During Metal Cutting

Eric P Whitenton
National Institute of Standards and Technology, 100 Bureau Drive, Gaithersburg MD, 20899-8223

ABSTRACT

Under certain conditions, the polarization state of infrared light emitted by metal changes when the metal is strained. During cutting, metal is severely strained. Assessing both strain and strain rate is of interest to the metal cutting research community. Over large areas, Digital Image Correlation (DIC) performed on high-speed video can provide approximate values for the average strain and strain rate. However, small areas such as the shear zone are difficult to image with enough resolution to perform DIC. If the thermal radiation emitted by these small areas is polarized, there is the potential to provide valuable information to the metal cutting community. This paper is an initial investigation into that possibility, as well as the use of the polarization information for uncertainty analysis, reflection detection, and region of interest classification. A rotating polarizer is used that triggers a thermal spectrum camera to acquire images at specific polarization angles. When cutting, the metal is constantly moving and the material imaged is different from one moment to the next. At each angle of the polarizer, a sufficiently long integration time is used so the material is severely motion blurred, resulting in an image which estimates the typical intensity for that angle. By comparing the typical intensities, and assuming the light is linearly polarized, the polarization state may be estimated.

Keywords: metal cutting, polarization, strain, high-speed imaging, infrared thermography

1. INTRODUCTION

Modeling is an important tool for optimizing manufacturing processes, allowing industry to make parts faster, better, and at less cost[1]. Measurements of the process using thermal[2-4] and visible[4-6] imaging can be used to improve and verify the accuracy of these models. The goals of manufacturing research at the National Institute of Standards and Technology (NIST) are to develop and improve measurement techniques, to develop an understanding of measurement uncertainties, to compare models of metal cutting to thermal and visible spectrum images to verify the models, and to share this understanding with the manufacturing community. To help achieve these goals, NIST developed a high-speed dual-spectrum imaging system MADMACS (the MAnufacturing Deformation MACro videography System)[7]. The manufacturing process studied in this paper is orthogonal metal cutting, where the edge of the cutting tool is perpendicular to the direction of workpiece motion. Figure 1 shows a schematic of a typical image. The relative motion between a cutting tool and a workpiece causes material to be removed from the workpiece. This removed material is referred to as a chip. Most of the deformation of the workpiece material occurs within a thin area called the shear zone.

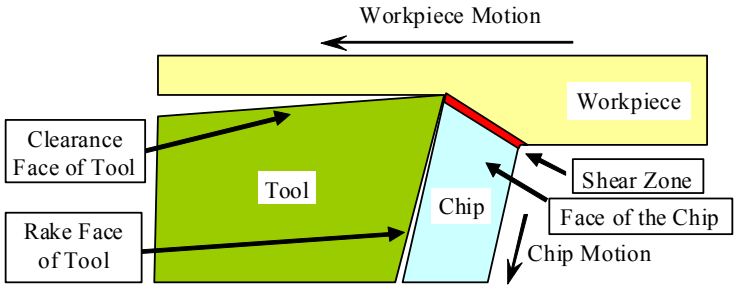

Figure 1. Schematic of an image of an orthogonal cutting process.

Thermosense: Thermal Infrared Applications XXXIII, edited by Morteza Safai, Jeff R. Brown,
Proc. of SPIE Vol. 8013, 801316 · © 2011 SPIE · CCC code: 0277-786X/11/$18 · doi: 10.1117/12.883453

The MADMACS system is calibrated using a blackbody which emits unpolarized thermal radiation. If the thermal radiation imaged during a measurement is 100 % polarized, the cold mirror (a specialized beam splitter) used in MADMACS causes a ±5 % variation in measured intensity as the polarization angle is varied. If the radiance temperature is 500 °C, the measured radiance temperature varies between 491 °C and 509 °C as the polarizer is rotated. This sensitivity to polarization is of no consequence if the thermal radiation imaged is unpolarized. However, if the thermal radiation has a significant polarized component, polarization would need to be taken into account in an uncertainty analysis of measurements produced by the system. This fact provided the initial motivation to measure the magnitude of polarization.

Properties associated with the thermal radiation emitted by a surface, such as emissivity, are significantly influenced by both the size and shape of surface features[8]. Surfaces, especially metal surfaces, can emit a significant amount of polarized light. When viewed on the macroscopic scale, this is often more pronounced for thermal radiation in the LWIR (long wave infrared, 8 µm to 12 µm wavelength) region than for the MWIR (mid-wave infrared, 3 µm to 5 µm wavelength) region[9,10]. MADMACS operates in the MWIR region. When viewed on the macroscopic scale, most surface features tend to scatter and depolarize emitted light[9,10]. However, viewing the surface on the macroscopic scale has the effect of averaging microscopic effects. MADMACS has a field of view of approximately 1 mm and sees the surface on a microscopic scale. When viewed on the microscopic scale, some features can significantly increase polarization. One example is a grating[11,12]. Another is a thin metal wire[13,14], where the polarization angle may be either parallel or orthogonal to the wire depending on width and temperature. It is interesting to note that emitted thermal radiation can also have a significant coherence length[15,16]. This could potentially produce interference effects in the thermal images. Blackbody radiation is not the only mechanism by which a surface may emit polarized light. Light from quantum wells such as certain light emitting diodes can be polarized due to strain[17-19]. Knowing the polarization state of emitted radiation on the microscopic scale can potentially yield information on the state of the surface. Metal cutting induces large strains in the material being machined, especially in the shear zone. These strains distort the surface being imaged, inducing structure to the surface. The potential for polarization to yield information related to material strain provides a second motivation for this work. The shear zone is so thin that measuring strain is difficult to do with other in-process techniques such as Digital Image Correlation.

Reflected thermal radiation is often polarized. Under the right conditions, this can be used to differentiate thermal radiation emitted by a surface from thermal radiation reflected by the surface[20]. During metal cutting, there are occasions when hot chips come between MADMACS and the surface being imaged. Thermal radiation emitted by these hot chips can sometimes be reflected off the surface being imaged and influence the perceived temperature. This is currently addressed by imaging the overall scene with a camcorder and throwing away tests when the chips go between the surface and MADMACS. Thus, a third motivation is the possibility of either detecting, or even correcting, measurements adversely affected by reflections without having to review the camcorder images.

A fourth and final motivation is the possibility of feature classification. When imaging metal cutting, there are three primary Regions Of Interest (ROI): the cutting tool, the chip, and the workpiece. Each ROI can move during a metal cutting operation, and has a dramatically different surface texture and emissivity. Currently, each ROI is detected manually so appropriate emissivity values may be applied to convert apparent temperature to true temperature. When processing large numbers of thermal images, the time spent performing this manual process can become significant. If polarization information could be used to help an automated image processing algorithm separate the ROIs in a robust way, the throughput of the overall measurement process would be significantly improved.

MADMACS, as modified for these polarization experiments, will be described next. Data obtained for heated stationary objects will then be presented. Finally, data obtained during metal cutting are given.

2. EQUIPMENT AND ANALYSIS METHODS

Figure 2 shows the MADMACS system, modified to perform the polarization experiments, imaging the orthogonal cutting of metal. The cold mirror has been removed. A holographic wire grid polarizer with an extinction ratio (the optical power parallel to the polarization angle divided by the optical power perpendicular to the polarization angle) of over 160 is mounted in a motorized rotational stage that rotates at 27.5 revolutions per second. The stage is equipped with a rotary encoder output and a home (once per revolution) output. The rotary encoder output is monitored by a processor board so that the thermal camera is triggered to capture images every 45° of the rotary stage. The home output is also monitored and used to orient the system so the same angle is used as 0° every time the system is used. The rotary stage is mounted in front of the primary lens.

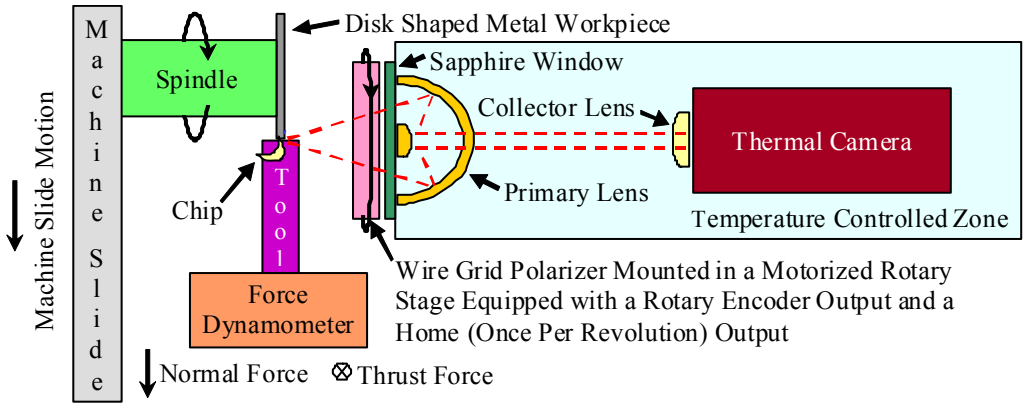

Figure 2. MADMACS system modified to perform polarization experiments. The modified MADMACS (on the right) is shown imaging the orthogonal cutting of metal.

If one assumes the polarization is linear, then S_3 of the Stokes vector is 0 and the following may be computed[21].

$$S_0 = I_0 + I_{90} \quad (1)$$

$$S_1 = I_0 - I_{90} \quad (2)$$

$$S_2 = I_{45} - I_{135} \quad (3)$$

$$T_u = \text{temperature corresponding to the intensity } (S_0 / 2) \quad (4)$$

$$DOP = 100\ \% \cdot (S_1^2 + S_2^2)^{1/2} / S_0 \quad (5)$$

$$A_m = \tfrac{1}{2} \cdot \arctan (S_2/S_1) \quad (6)$$

$$A_I = F(A_m) \quad (7)$$

Where I_0, I_{45}, I_{90}, and I_{135} are the intensities measured at the rotary stage angular coordinates 0°, 45°, 90°, and 135°, respectively. S_0, S_1, and S_2 are elements of the Stokes vector. T_u is the temperature which corresponds to the intensity measured by a camera which is not sensitive to polarization. DOP is the degree of polarization expressed as a percentage. A_m is the measured angle of polarization in the coordinate system of the rotational stage. A_I is the angle of polarization transformed to correspond to the coordinate system of the images, and is bound between 0° and 180°. The rotary stage angular coordinates of 0 °, 45 °, 90 °, and 135 ° correspond to the image angles of 110°, 65°, 20°, and 155°, respectively. An image angle of 0° is horizontal in the images. An image angle of 90° is vertical in the images. Except for Table 1, image angle coordinates are the only angular coordinates referenced in the remainder of this paper.

The system is calibrated by imaging a blackbody over a range of temperatures with the polarizer at the various angles used. The calibration yields a set of calibration curves for each pixel in the thermal image relating intensity and polarizer angle to apparent temperature. MADMACS has a working distance (the distance from the front of the primary lens to the surface being imaged) of approximately 2 cm. Unfortunately, the rotary stage is approximately 1.5 cm thick. Thus, the effective working distance of the modified MADMACS is only about 0.5 cm. The blackbody used to calibrate

MADMACS is constructed such that the system can not come closer than about 1.5 cm to the opening of the blackbody. Thus, the system was calibrated using out-of-focus images of the blackbody which have reduced intensities. For these experiments, we are concerned only with relative changes in intensity as the polarizer rotates. Thus, while the measured temperatures of the resulting images are incorrect, the computed polarization information is correct.

To verify that the system performs properly, a second holographic wire grid polarizer was placed in front of the blackbody and imaged. Since the working distance for the modified MADMACS is so short, precision rotational positioning of this second polarizer was not practical. Table 1 shows results for several positions of the second polarizer. Comparing the approximate positions of a second polarizer to measured values verify system is performing properly.

Table 1. Comparing approximate positions of a second polarizer to measured values.

Approximate Position of Second Polarizer	Measured Angle (A_M)	Measured Degree of Polarization (DOP)
0°	-3.0°	95.8 %
45°	45.0°	97.3 %
90°	91.4°	95.9 %
135°	138.5°	96.7 %

3. POLARIZATION IN IMAGES OF STATIONARY HEATED OBJECTS

3.1 Thermal Vise

To heat stationary objects, a thermode heater controller was used. It is capable of supplying an adjustable voltage, up to 3.8 volts, and up to 4 kW of power. It monitors a thermocouple and adjusts the voltage to hold a constant temperature. The heater control was connected to a thermal vise, which holds the objects to be heated. The thermal vise is a machinist vise modified by adding a pair of non-conductive phenolic strips and a pair of conductive copper strips. Figure 3a shows the thermal vise. The rest of the figure shows various objects to be heated, which will be discussed next.

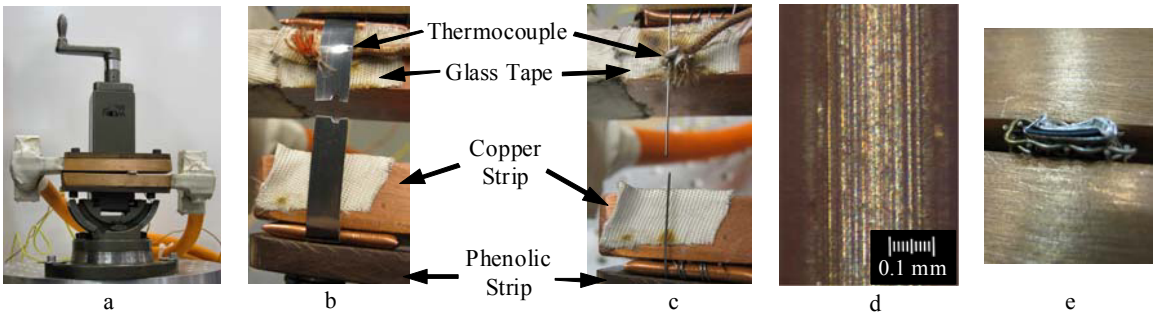

Figure 3 Figure 3a shows the thermal vise. Figure 3b shows the thermal vise used to measure the response of nichrome ribbon. Figure 3c shows the thermal vise used to measure the response of nichrome wire. Figure 3d shows a micrograph of the wire. Figure 3e shows the thermal vise used to measure the response of a metal chip protruding from a wrapping of aluminum foil which is wrapped in nichrome wire mesh; the thermocouple is buried in the aluminum foil, pressed against the chip.

3.2 Nichrome Ribbon and Nichrome Wire

Nichrome has a high resistivity compared to most metals. When placed in the thermal vise, the high resistivity causes the nichrome to absorb most of the electrical energy output by the controller, making nichrome a convenient and efficient heating element. To see if stress, strain, or the resulting surface deformation induces a change to the polarization state of thermal radiation emitted by nichrome, nichrome ribbon and nichrome wire were mounted in the thermal vise and strained by opening the vise until the samples broke. Examples are shown in Figure 3b and Figure 3c respectively. Two

ribbons were evaluated, one was 20 µm thick while the other was 46 µm thick and had a hole punched to control the failure location. The thermal data, not shown, indicates no significant change in the polarization state as the ribbons were strained.

A 0.4 mm diameter (26 gauge) nichrome wire was evaluated next, shown in Figure 3c and Figure 3d. The wire was likely made by a drawing or extrusion process, and ridges along the length of the wire are clearly observed. Figure 4a shows results with no force applied by the vise. Figure 4b shows results with the wire being pulled by opening the vise, and was acquired just before the wire broke. The left hand column in Figure 4a and Figure 4b shows images measured at different angles of the polarizer. The right hand column shows results computed using Equation 1 through Equation 7. The wire is not perfectly vertical in the images, and is oriented to the right. The degree of polarization is the largest along the sides of the wire, which has a steep overall slope. These images were acquired several centimeters from the thermocouple, and the measured temperature changed as the wire was pulled. Unfortunately, Figure 4a and Figure 4b image different locations of the wire. It is not clear whether the slight difference is simply due to surface variation along the wire.

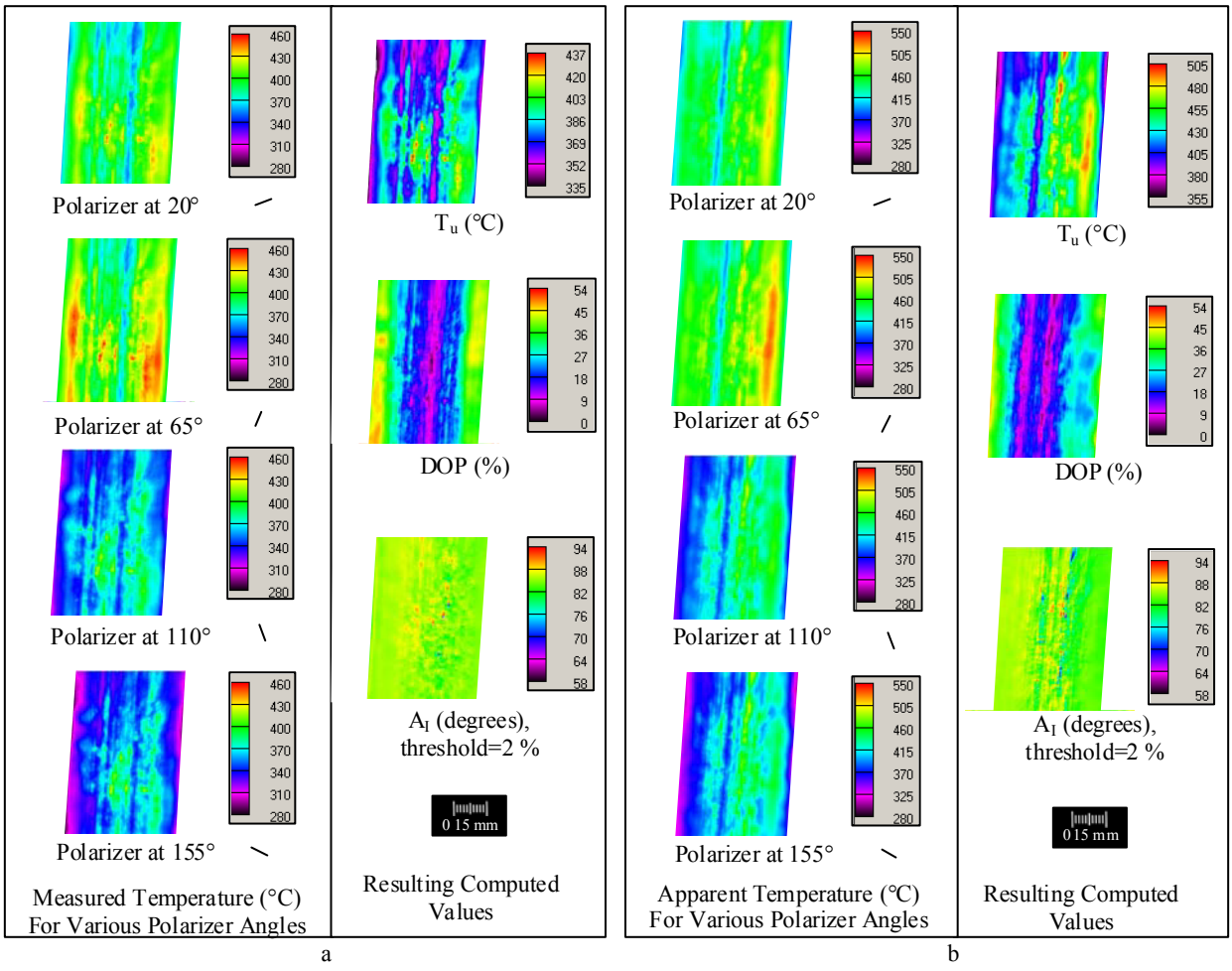

Figure 4 Figure 4a shows nichrome wire with no added strain. Figure 4b shows nichrome wire tensioned to near the breaking point. The severely out-of-focus portions of the images are masked. Measured temperatures are shown on the left in each figure and the computed results are shown on the right in each figure. Each pixel in the A_I image is only shown if the corresponding DOP has a value greater than 2 %. For all false color images, any pixel with a value outside the range indicated is white in the image.

3.3 Ground and Polished Tool

NIST sometimes images the cutting tool during metal cutting to determine tool temperature. To accomplish this, the side of the tool is ground flat. Shown in Figure 5a, the average DOP is about 4 %. The A_I is approximately parallel to the 100° grinding marks. Figure 5b shows the same tool which has been rubbed with successively finer abrasive papers down to 1200 grit. The flat portion of the tool emits less polarized radiation while the rounded edges of the tool emit more. Images of the tool were also taken with a hot soldering iron in front of the tool, and the thermal radiation reflected off of the tool was not significantly more or less polarized than the light emitted by the tool.

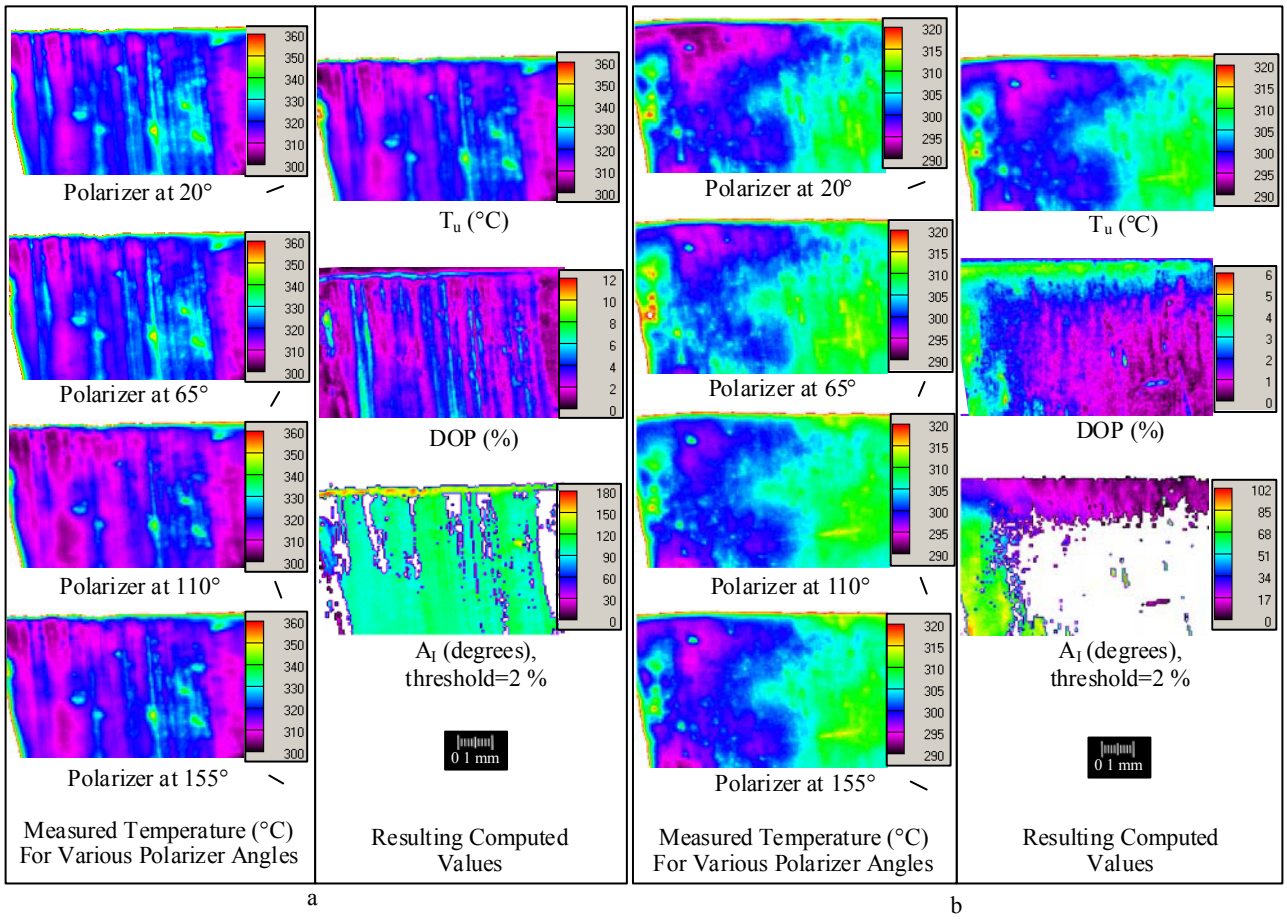

Figure 5 Figure 5a shows the ground side of a carbide cutting tool. Figure 5b shows the same tool rubbed with successively finer abrasive papers down to 1200 grit. The edges of the tool are rounded due to the rubbing with the abrasive papers. The cutting edge is to the left in the images, just out of the field of view. Each pixel in the A_I image is only shown if the corresponding DOP has a value greater than 2 %. For all false color images, any pixel with a value outside the range indicated is white in the image.

3.4 Metal Cutting Chips

Chips from metal cutting tests may be heated as shown in Figure 3e and imaged. Chips can be can be classified according to their shapes. Figure 6 and Figure 7 shows an example of a serrated chip, which has a saw tooth shape. The inconel chips have significant side flow. Side flow is where metal has flowed toward the camera during metal cutting and protrudes beyond the side of the chip. The DOP image in Figure 7 shows the faces of the chip are about 3 % polarized while the edges of the faces are over 7 % polarized.

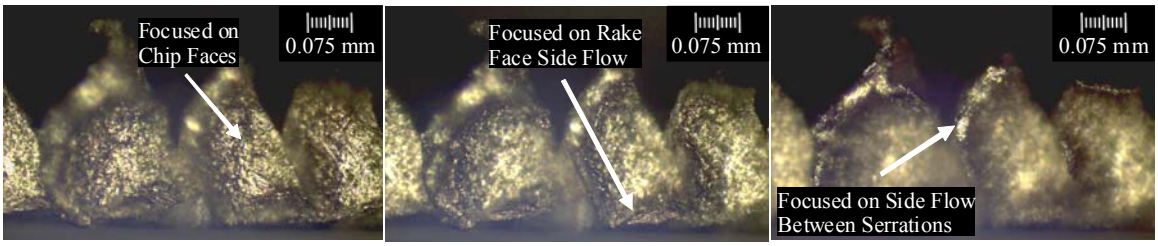

a b c

Figure 6 Visible light images of a serrated inconel chip which has a significant amount of side flow. Figure 6a is focused on the faces of the chip. Figure 6b is focused on the side flow from the bottom of the chip, which was along the rake face of the tool during cutting. Figure 6c shows side flow from the sides of the serrations, which protrude the farthest from the face of the chip.

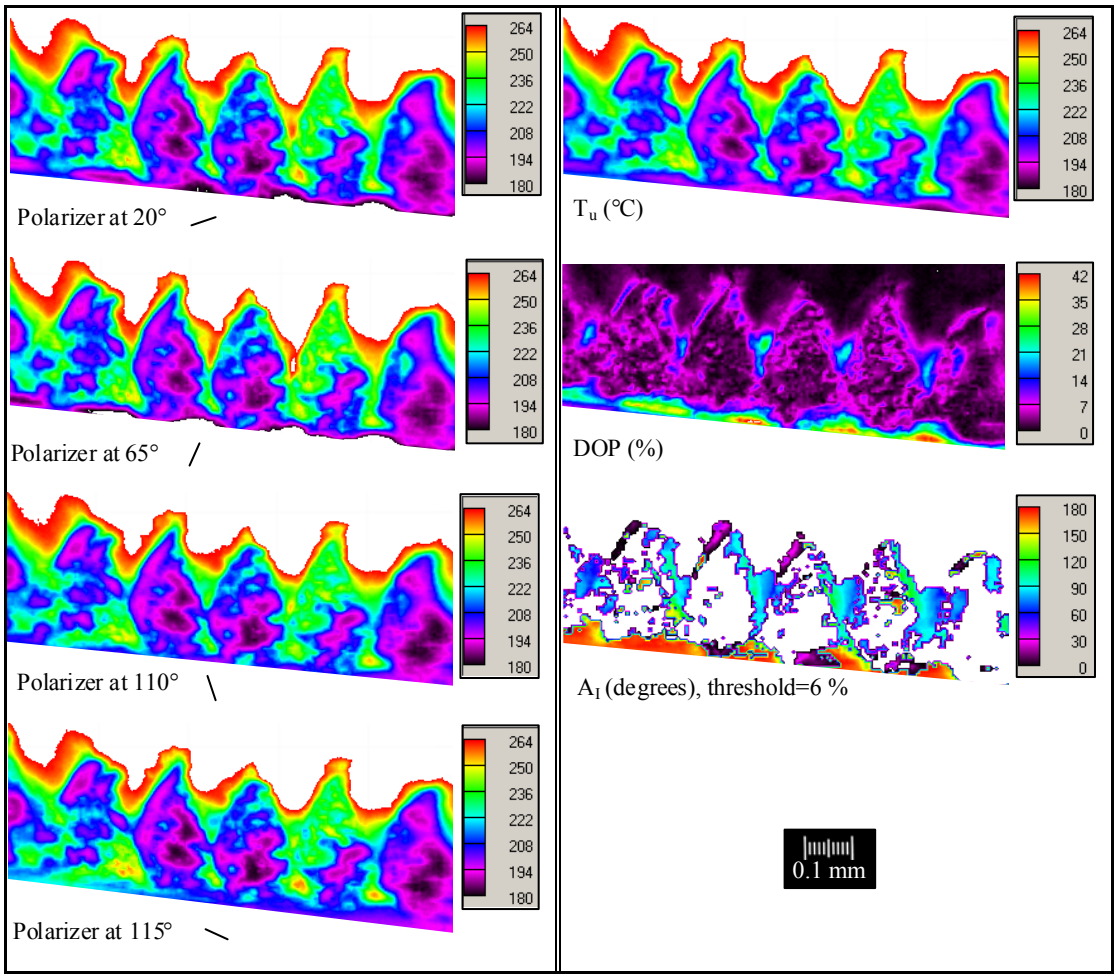

Figure 7 Thermal images of an inconel chip. Each pixel in the A_I image is only shown if the corresponding DOP has a value greater than 6 %. For all false color images, any pixel with a value outside the range indicated is white in the image.

Figure 8 and Figure 9 show relatively planar steel chips. As is often the case, in some locations the chips have a serrated shape while other portions have a stacked brick shape. The DOP image in Figure 9 shows the faces of the segments are only a few percent polarized while both the edges of the segments and the side flowed portions are significantly polarized, in some cases over 20 %.

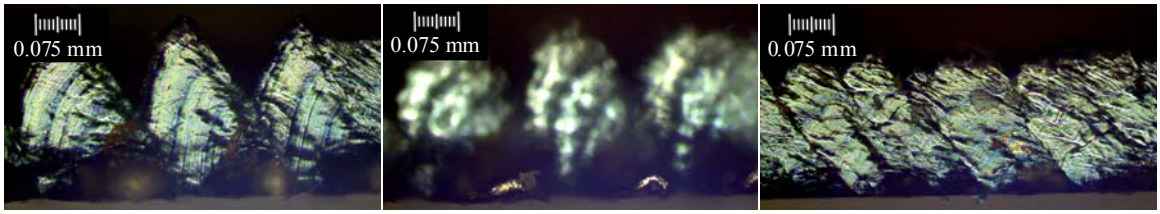

a b c

Figure 8 Visible light images of steel chips. Figure 8a shows that the serrations are relatively planar, except for occasional small side flows along the bottom (Figure 8b). As is often the case, in some locations the chip has a serrated shape while other portions have a stacked brick shape, shown in Figure 8c.

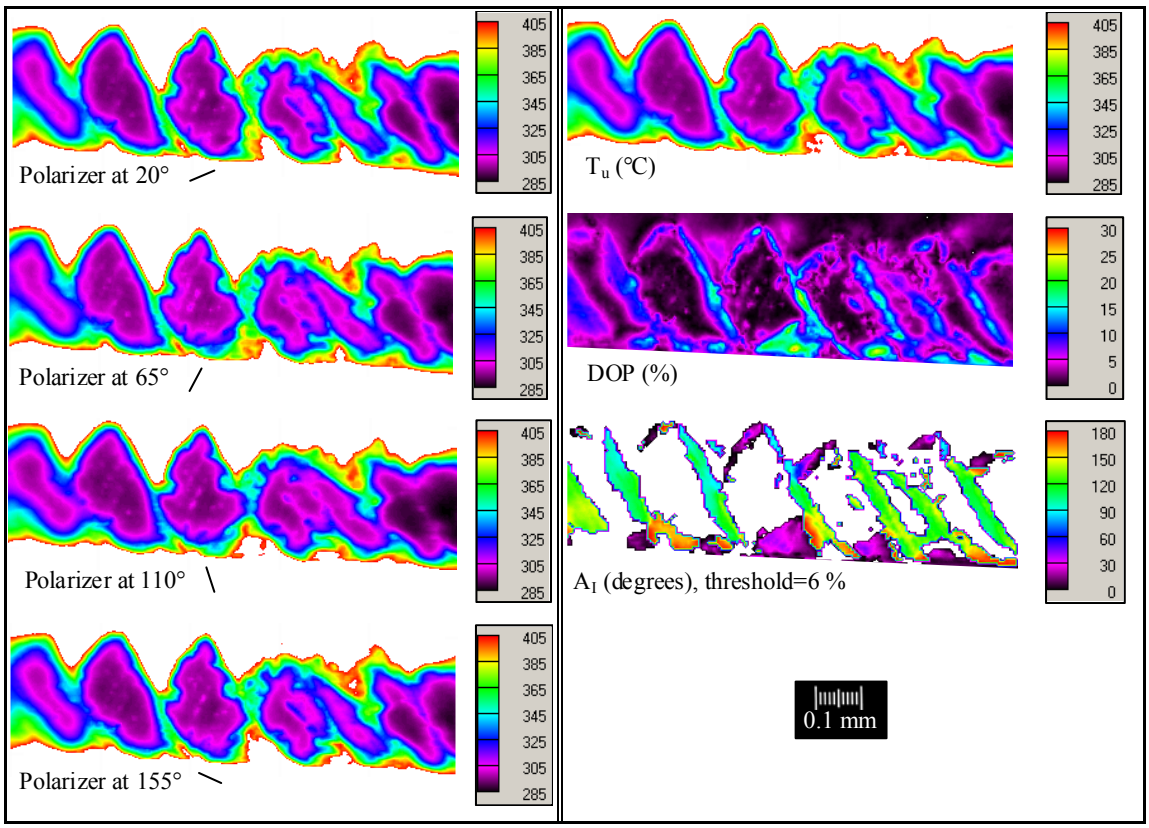

Figure 9 Thermal images of a steel chip. Some segments of the chip have a serrated shape while other segments have a stacked brick shape. Each pixel in the A_I image is only shown if the corresponding DOP has a value greater than 6 %. For all false color images, any pixel with a value outside the range indicated is white in the image.

Figure 10 and Figure 11 also show steel chips. However, the workpiece had received a different heat treatment, different surface preparation, and was machined using different cutting parameters than the chips shown previously. The chips have a relatively uniform stacked brick shape, and the faces of the chips have a relatively uniform striation pattern parallel to the sides of the "bricks." This produces a consistent thermal emission of light which is about 19 % polarized, with A_I parallel to the striations.

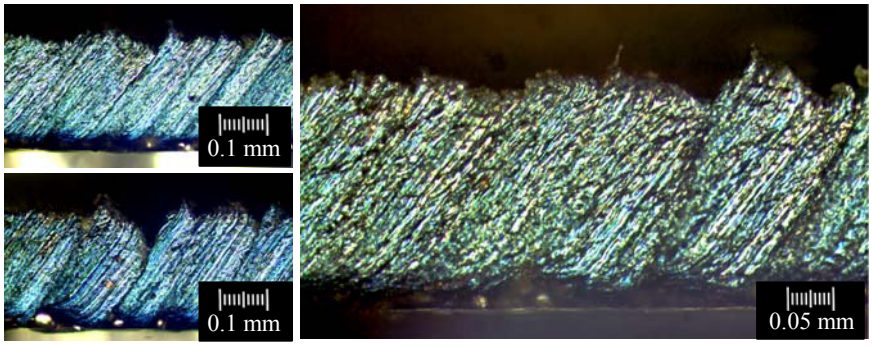

Figure 10 Visible light images of steel chips.

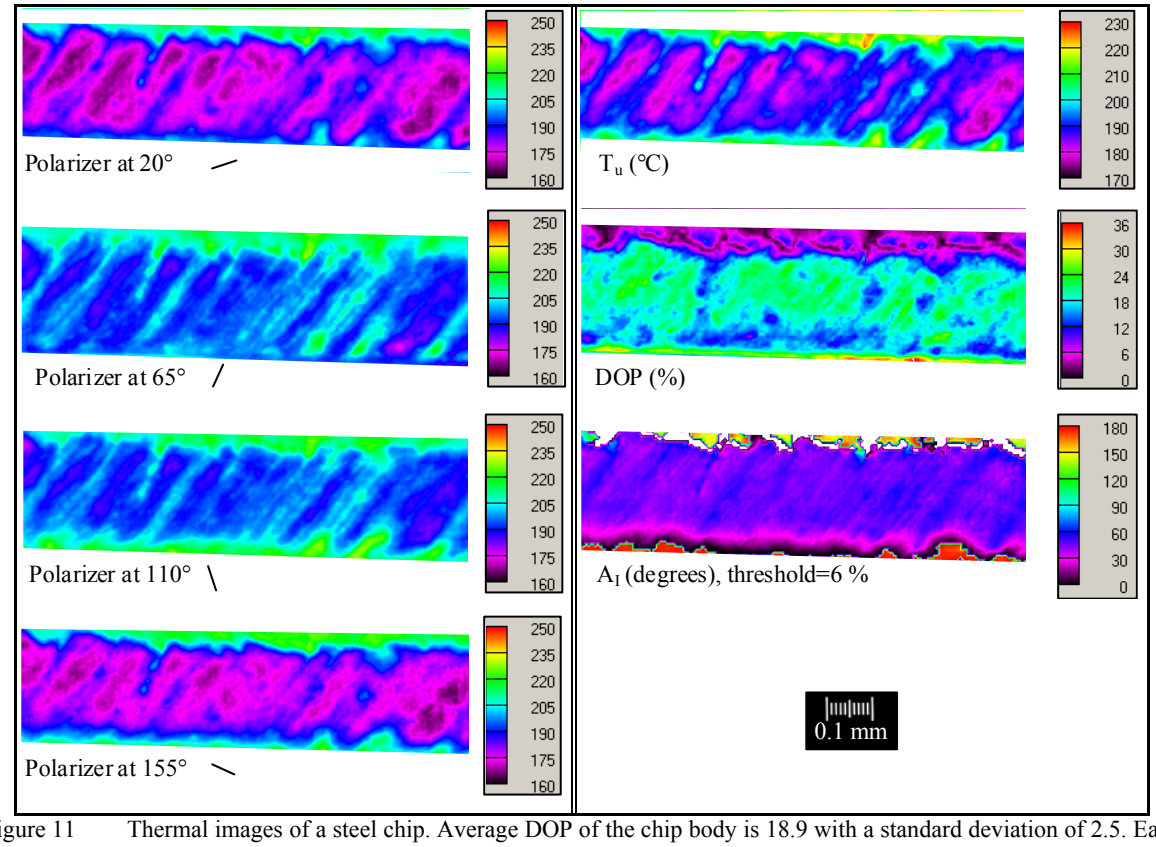

Figure 11 Thermal images of a steel chip. Average DOP of the chip body is 18.9 with a standard deviation of 2.5. Each pixel in the A_I image is only shown if the corresponding DOP has a value greater than 6 %. For all false color images, any pixel with a value outside the range indicated is white in the image.

Figure 12 and Figure 13 show another set of steel chips produced in a similar, though not exactly the same, manner as the chips in Figure 10 and Figure 11. Note how the striations on the face of the chips are much less regular. In this case, the DOP is only about 6 %, as compared to 19 % for the chips in Figure 10 and Figure 11. Images of several heated chips were also taken with a hot soldering iron in front of the chips. The thermal radiation reflected off the chips was not significantly more or less polarized than the light emitted by the chips.

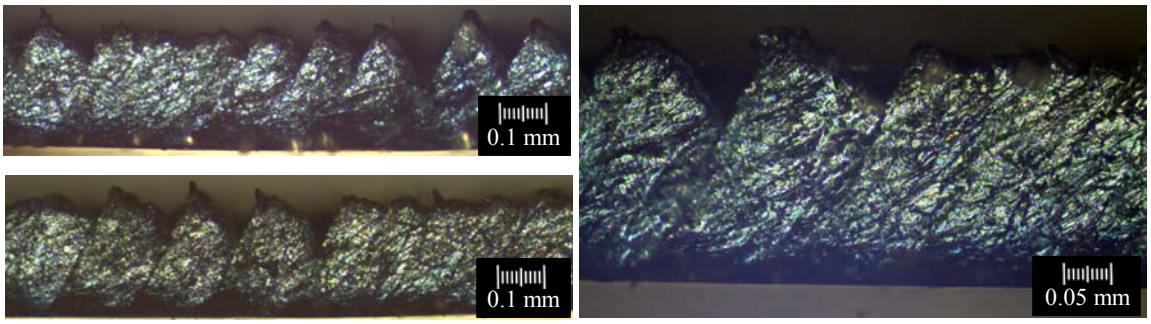

Figure 12 Visible light images of steel chips.

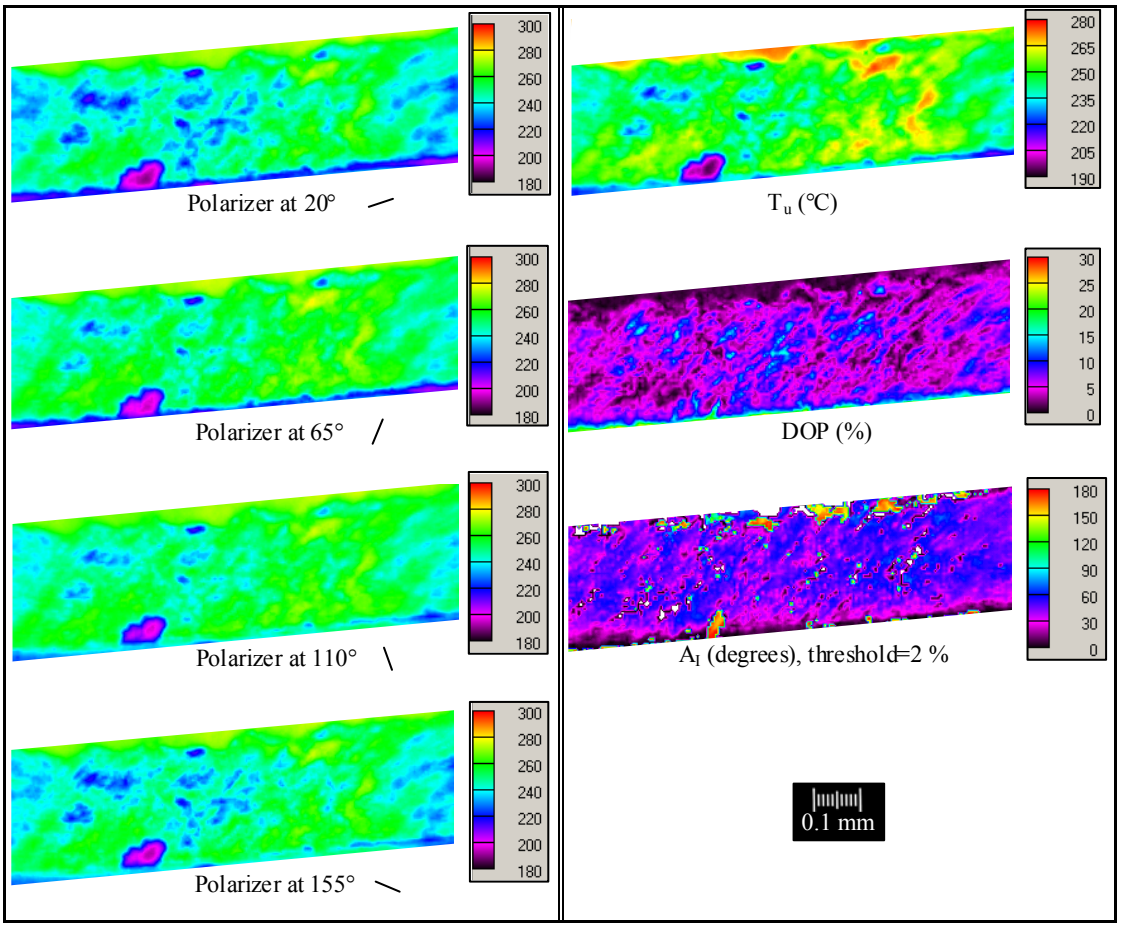

Figure 13 Thermal images of a steel chip. Average DOP of the chip body is 6.0 with a standard deviation of 2.8. Each pixel in the A_I image is only shown if the corresponding DOP has a value greater than 2 %. For all false color images, any pixel with a value outside the range indicated is white in the image.

4. IMAGES OF METAL CUTTING

Figure 14 shows thermal images taken during the metal cutting test which produced the chips shown in Figure 12 and Figure 13. The main features in Figure 14 correspond to those in Figure 1. No coolants or cutting lubricants were used. The images on the left are raw thermal camera images acquired using a short, 9 µs integration time so as to minimize motion blur. However, with such a short integration time, the non-uniformity in the images is so severe that they are useful for qualitative purposes only.

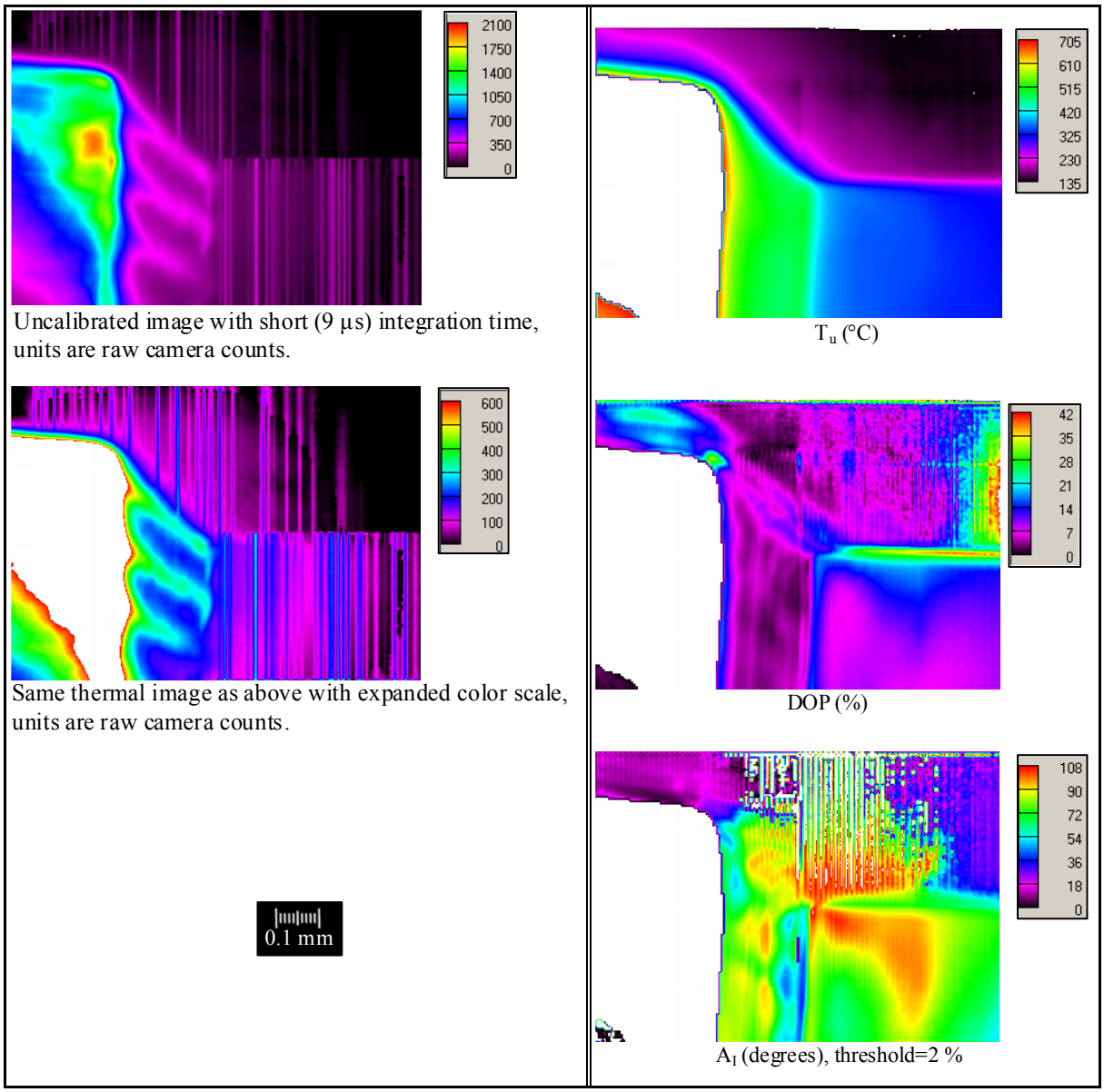

Figure 14 Steel being machined. The resulting chips were shown in Figure 12 and Figure 13. The left hand side shows short integration time images which minimize motion-blur, but only yield qualitative images. The measured images used to generate the right hand side, which had relatively long integration times, are not shown. Average DOP of the chip body is 4.1 with a standard deviation of 0.9. Each pixel in the A_I image is only shown if the corresponding DOP has a value greater than 2 %. For all false color images, any pixel with a value outside the range indicated is white in the image.

The images used to produce the polarization analysis on the right were acquired using a 180 μs integration time and are severely motion blurred. The shear zone shows a higher DOP than the body of the chip. A polarization of about 4 % in the body of the chip was measured. This is lower than the 6 % polarization measured for the body of the chip in Figure 13. This difference is likely due to several factors. First, there is variability between different portions of the chip, which are averaged together by using the long integration time. Second, the chip in Figure 14 is very hot while in the field of view, and the shape may change somewhat as the chip cools. Thus, a chip imaged after a test might not have exactly the same shape it had while in the field of view of the thermal camera. Third, looking at the left hand images in Figure 14, notice that the chip is not uniformly heated. The chip along the rake face of the tool, as well as the gaps between the segments (or "bricks"), are significantly hotter than the faces of the chip. Thus, the 180 μs integration time images are measuring a weighted average where the hotter portions of the chip have a higher weight than the cooler, less bright portions. Fourth, it is conceivable that DOP may vary with surface temperature. The overall temperature of the chip in the thermal vise is lower than it was during machining.

5. CONCLUSIONS

Four motivations for these experiments were discussed in the introduction. Based on the results of these preliminary experiments, the following conclusions may be drawn:

The normal configuration of MADMACS has ±5 % variation in measured intensity if the thermal radiation is 100 % polarized. Under the right circumstances, segment faces can emit 20 % polarized thermal radiation, yielding an approximate Type B, k=2, uncertainty[22] in measured intensity of about 1 % due to polarization effects. Side flow and the edges of chip serrations can have significantly higher polarization, and thus a higher uncertainty. The cutting tool rarely showed polarization above 6 %, which introduces a Type B, k=2, uncertainty of about 0.3 % in measured intensity. The uncertainty in temperature which results from uncertainty in measured intensity depends on both the temperature and the emissivity of the object being measured. For example, when the measured radiance temperature is 500 °C, and emissivity is 0.8, a 1 % deviation in measured intensity produces a 2 °C deviation in computed true temperature. For most situations experienced in metal cutting, the Type B, k=2 uncertainty is generally 3 °C or less. This information can be used in future uncertainty estimates for MADMACS results.

The second, and perhaps most important, motivation was to explore if polarization could yield information that may be related to material strain. Figure 14 shows an elevated polarization level in the shear zone. However, more experiments are needed to differentiate between the amount of strain and the effect of the shapes of surface features induced by the strain. Are we measuring the amount of strain, the shape of the strain, or a combination of both? In addition, using a LWIR camera may work much better than our MWIR camera.

The third motivation was to explore the possibility of either detecting or correcting measurements adversely affected by reflections. No evidence supporting this was found. It may be that these surfaces are too rough for this to work on the microscopic scale.

The final motivation was that of differentiation between different regions of interest. Since the polarization of thermal radiation emitted by the cutting tool is determined by the surface finish of the tool, one could select a surface finish that emits thermal radiation with a different polarization state than the chip, facilitating robust automated differentiation between the tool and chip. Also, some types of chips emit more polarized thermal radiation than others. It may be possible to create a real-time sensor that measures the polarization state of the thermal radiation emitted by the chip to determine what type of chip is being produced.

ACKNOWLEDGEMENTS

The author wishes to acknowledge Robert Ivester, Johannes Soons, and Howard Yoon of the National Institute of Standards and Technology.

REFERENCES

1. R. W. Ivester and J. C. Heigel, "Smart Machining Systems: Robust Optimization and Adaptive Control Optimization for Turning Operations," Transactions of the North American Research Institute (NAMRI)/SME **35**, 505-511 (2007).
2. E. P. Whitenton, R. W. Ivester, and H. Yoon, "Simultaneous Visible and Thermal Imaging of Metals During Machining," SPIE Proceedings **5782**, 71-82 (2005).
3. J. C. Heigel, R. W. Ivester, and E. P. Whitenton, "Cutting Temperature Measurements of Segmented Chips using Dual-Spectrum High-Speed Microvideography," Transactions of the North American Research Institute (NAMRI)/SME **36**, 73-80 (2008).
4. E. P. Whitenton, "High-Speed and Dual-Spectrum Videos of Machining Processes," web link **http://www nist.gov/el/isd/sbm/hsds-machining-videos.cfm**, (2010).
5. E. P. Whitenton, J. C. Heigel, and R. W. Ivester, "Measurement and Characterization of Dynamics in Machining Chip Segmentation," 11th CIRP International Workshop on Modeling of Machining Operations 237-246 (2008).
6. R. W. Ivester, E. P. Whitenton, J. C. Heigel, T. Marusich, and C. Arthur, "Measuring Chip Segmentation by High-Speed Microvideography and Comparison to Finite-Element Modeling Simulations," 10th CIRP International Workshop on Modeling of Machining Operations 37-44 (2007).
7. E. P. Whitenton, "High-Speed Dual-Spectrum Imaging for the Measurement of Metal Cutting Temperatures," National Institute of Standards and Technology **NISTIR 7650**, (2010).
8. F. Ghmari and T. Ghbara, "Influence of Microroughness on Emissivity," Journal of Applied Physics **96**, 2656-2664 (2004).
9. G. Forssell and E. Hedborg-Karlsson, "Measurements of Polarization Properties of Camouflaged Objects and of the Denial of Surfaces Covered with Cenospheres," SPIE Proceedings **5075**, 246-258 (2011).
10. K. P. Gurton, R. Dahamani, and G. Videen, "Measured Degree of Infrared Polarization for a Variety of Thermal Emitting Surfaces," Army Research Laboratory **ARL-TR-3240**, (2004).
11. F. Marquier, C. Arnold, M. Laroche, J. J. Greffet, and Y. Chen, "Degree of Polarization of Thermal Light Emitted by Gratings Supporting Surface Waves," Optics Express **16**, 5305-5313 (2008).
12. J. H. Lee, W. Leung, T. G. Kim, K. Constant, and K. M. Ho, "Polarized Thermal Radiation by Layer-By-Layer Metallic Emitters with Sub-wavelength Grating," Optics Express **16**, 8742-8747 (2008).
13. G. Bimonte, L. Cappellin, G. Catugno, G. Ruoso, and D. Saadeh, "Polarized Thermal Emission by Thin Metal Wires," New Journal of Physics **11**, (2009).
14. L. J. Klein, S. Ingvarsson, and H. F. Hamann, "Changing the Emission of Polarized Thermal Radiation from Metallic Nanoheaters," Optics Express **17**, 17963-17969 (8009).
15. J. J. Greffet, R. Carminati, K. Joulain, J. P. Mulet, S. Mainguy, and Y. Chen, "Coherent Emission of Light by Thermal Sources," Nature **416**, 61-64 (2002).
16. J. Ginn, D. Shelton, P. Krenz, B. Lail, and G. D. Boreman, "Polarized Infrared Emission using Frequency Selective Surfaces," Optics Express **18**, 4557-4563 (2010).
17. H. Masui, H. Asamizu, A. Tyagi, N. Fellows DeMille, S. Nakamura, and S. P. DenBaars, "Correlation between Optical Polarization and Luminescence Morphology of (1122)-Oriented InGaN/GaN Quantum-Well Structures," Applied Physics Express **2**, 071002-1-071002-3 (2009).
18. J. Shakya, K. Knabe, K. H. Kim, J. Li, J. Y. Lin, and H. X. Jiang, "Polarization of III-Nitride Blue and Ultraviolet Light-Emitting Diodes," Applied Physics Letters **86**, 091107-1-091107-3 (2005).
19. M. Cooke, "Polarized LED from RPI and Kyma Promises More Efficient Displays," Semiconductor Today **5**, 112-113 (2010).
20. M. Vollmer, S. Henke, D. Karstädt, K. P. Möllmann, and F. Pinno, "Identification and Suppression of Thermal Reflections in Infrared Thermal Imaging," InfraMation 2004 Proceedings **5**, 287-298 (2004).
21. R. Distl and T. Egeler, "Polarization Measurement of Light Radiation," Instrument Systems GmbH (1988).
22. B. Taylor and C. Kuyatt, "Guidelines for Evaluating and Expressing the Uncertainty of NIST Measurement Results," National Institute of Standards and Technology **Technical Note 1297**, (1994).